Dianne I. Greenfield, PhD. CUNY Advanced Science Research Center & Queens College
Final Report: Elucidating linkages between storm events and microbial assemblage diversity in the Lower Hudson River through genomic and biogeochemical analysis: Implications for climate and water quality forecasts

Abstract:

Aquatic microbes are incredibly diverse, reflecting a vast array of essential ecological and biogeochemical functions such as photosynthesis, respiration, and nutrient cycling. The urban microbiome is an excellent indicator of water quality and human impacts. This study assessed linkages between wet weather presumably associated with combined sewer overflow (CSO) discharge and the water quality of the Lower Hudson River Estuary (HRE), emphasizing Piers 26 and 51 within the Hudson River Park Trust. Key physical, biogeochemical, and microbial parameters were measured bi-weekly July-October 2023 and in response to storm events. Findings showed that nitrogen in the form of ammonium, a nutrient associated with wastewater, was considerably elevated throughout the sampling period. This was accompanied by heightened water turbidity across the study duration. Co-occurring phytoplankton species were typically diatoms, with low overall biomass and diversity. Harmful algal bloom (HAB) forming dinoflagellates were detected during the fall, including elevated levels of toxin-producing *Prorocentrum* species. Bacterial abundances spiked following intense rainfall, suggesting a response to wastewater inputs (growth and discharge). These findings shed novel insight on the HRE ecosystem as results indicate that the microbiome may be co-stressed by ammonium and light limitation rather than driven primarily by a single factor (such as light). While elucidating the precise mechanisms warrant further research, results herein provide critical baseline data for future research, climate modeling, and NYC coastal water quality management.

Introduction:

Aquatic microbes (phytoplankton, Archaea, bacteria, other protists) have extraordinary genetic diversity reflecting a vast array of ecological and biogeochemical roles. As examples, phytoplankton generate ~50% of the world's oxygen through photosynthesis, and microbial communities facilitate vital processes such as respiration, nutrient and greenhouse gas transformation, and metabolism. Due to their short generation times (hours-days), microbes are highly responsive to fluctuations in surrounding conditions and environmental change.

The urban microbiome is an excellent indicator of water quality and human impacts (Herve et al. 2018). For example, the Lower Hudson River Estuary (HRE) receives excessive nutrient (primarily nitrogen, N) loading from agricultural, industrial, and residential landscapes associated with the New York City (NYC) metropolitan area. A major source of HRE contamination is fecal coliform and N-rich wastewater from combined sewer overflows (CSOs) associated with storm events (Steinberg et al. 2004; Wang 2014; Riverkeeper 2015; HEP 2020). The HRE is hydrologically connected to NYC's Upper Bay as well as the East River, with N loading contributing to algal bloom formation in nearby embayments as well as summer hypoxia from microbial respiration of organic matter (e.g., sewage, phytoplankton) alongside environmental forcings (Vaudrey 2017; Whitney and Vlahos 2021; Humphries et al. 2023).

Since climate change is predicted to increase storm frequency and intensity, particularly in low elevation cities like NYC (IPCC 2018), elucidating linkages between microbial abundances and community composition, and therefore presumably ecosystem function, CSO discharge, and precipitation is a critical public health need. **We hypothesized that wet weather (rainfall, storms) associated with CSO discharges will result in lower microbial biomass, abundances, and diversity than dry weather** such that wet scenarios may reduce ecological function. New

York City has an antiquated sewer system with 700 CSOs, and ~32 of them in Hudson River Park (henceforth 'the Park'), that release untreated wastewater to the Lower HRE following precipitation, creating the ideal urban setting to test this hypothesis. Accordingly, using the Park as our study region, we combined microbial and biogeochemical analyses to elucidate associations between the urban microbiome, eutrophication, and climate-relevant impacts (storms/precipitation). By comparing microbial assemblages between wet and dry time frames, one can inform public health 'risk assessments' associated with CSO events in the Park, thereby establishing a critical baseline for future work wherein long term databases and sample collections can be leveraged to validate climate and water quality models. For this project, we defined 'wet' time frames as periods when cumulative 5-day precipitation was >15 mm and 'dry' time frames as periods of ≤15 mm cumulative 5-day precipitation. Within that context, project **objectives** were to (**1**) determine the influence of CSO inputs (as 'wet' vs. 'dry' conditions) on key physical water quality and biogeochemical parameters; (**2**) assess microbial biomass, abundances, and diversity as they relate to 'wet' and 'dry' conditions.

Methods:

Sample Collection and Physical Water Quality. Surface (0.2 m depth) water was sampled 2x per month from 18 July to17 October 2023 during mid-ebb tide from two piers within the Park boundary to capture nutrients, bacteria, and phytoplankton flowing from the Hudson River toward the Upper Bay of the Hudson River Estuary (HRE). Pier 26 (40.7209201, -74.0131924) was sampled from a floating dock on the south of the pier, and Pier 51 (40.7382976, -74.0108394) was sampled from an observation deck (~5 m above the water's surface) on the northwestern corner of the pier. On 18 July, Gansevoort Peninsula (henceforth GV) (40.739729, -74.012202) was sampled

along the south side of the pier with Pier 26, but GV was subsequently replaced by the neighboring Pier 51 due to construction creating a hazardous setting (**Figure A1**). In addition to our regular surveillance, we intensified our sampling frequency mid-September in response to a storm event. This entailed sampling on 14, 15, and 20 September during a period when total precipitation was ~60 mm as well as another date (3 October) added to capture a second rainy period when 5-day cumulative precipitation was ~37 mm (**Table A1**). This strategy allowed us to address our over-arching study goal of comparing 'wet' and 'dry' timeframes.

For each site and sampling date, surface depth physical water quality (temperature (T, ^{o}C), salinity (S, dimensionless), and dissolved oxygen (DO, mg/L)) was measured using a hand-held YSI ProSolo sonde, and Secchi depth (m) measurements were used to calculate light extinction coefficients (k) (Beer's Law) as k = 1.7/(Secchi depth). Data for pH and precipitation were leveraged from the Hudson River Ecosystem Conditions Observing System (HRECOS; https://hrecos.org/) located at Pier 25 (adjacent to Pier 26). We realize that cloud bursts can cause sudden and hyper-localized flooding in NYC (Rosenzweig et al. 2024), though for the purposes of this pilot study we assumed that precipitation conditions at Piers 26 and 51 were comparable. At Piers 26 and GV, water samples were collected directly (elbow grab) using a previously acid-washed (10% hydrochloric acid, HCl, for ≥4 h then rinsed 3x with reverse osmosis (RO) water followed by analytical-grade distilled water (DI) rinse) 2 L brown high-density polyethylene Nalgene® bottles. At Pier 51, samples were collected by a Park staff member lowering a plastic bucket from the observation deck. River water was then dispensed in to 2 L Nalgene® bottles. On 18 July, 16 August, 15 September, and 3 October, water samples were collected as above but using previously acid-washed 9 L polycarbonate carboys instead of 2 L bottles to allow enough volume for genomic sample processing. All samples were placed in a cooler with cold packs then

immediately transported to the laboratory. Upon return to the laboratory, all sample bottles were gently rotated 10x to ensure the contents were well-mixed then subsampled in triplicate for nutrients, bacteria, and phytoplankton as follows.

Nutrient Analysis. Upon return to the laboratory, water (~17 ml) from each replicate was passed through previously acid-washed (as above) 60 mL syringes affixed with 0.7 μm, 25 mm diameter glass microfiber filters (GF/Fs) (Whatman™ Cytiva, product #1825-025) into acid washed 20 ml glass scintillation vials for analysis of ammonia+ammonium, nitrite+nitrate, and orthophosphate. Dissolved silicate was similarly processed, but into plastic scintillation vials. All samples were frozen (-20 °C) until colorimetric analysis using a Lachat Quickchem® 8500 autoanalyzer following standard wet chemistries of marine samples (Grasshoff et al. 1999; Hales et al. 2004).

Bacterial Abundances. Site water was initially passed through a 20 μm Nitex® mesh to exclude larger particles. Filtrate (27 ml) was dispensed into 50 ml amber glass vials containing 3 ml of 20% Phosphate-buffered saline (PBS) buffered formaldehyde that was added no more than 1 h beforehand (final concentration of 1.13% PBS), then fixed samples were stored at 4 ˚C. Detailed procedures for preparing PBS stock and working solutions may be found in Humphries et al. (2023). Thermo Fisher Scientific™ 4′,6-diamidino-2-phenylindole (DAPI) stock solution was prepared by diluting 1 mg of DAPI/1 ml double-distilled water (ddH_2O), with working solution then prepared as 100 μl DAPI stock/1 ml ddH_2O for a 10,000 μg/1 ml ddH_2O final concentration (Porter and Feig 1980). Bacterial cells were stained with DAPI on to Isopore™ 0.2 μm black polycarbonate membrane filters, mounted on to glass slides, then stored (-20 ˚C) in the dark until analysis using a Nikon ECLIPSE Ni upright epifluorescent microscope (DAPI excitation peak at 259 nm and emission peak at 457 nm) at 400x magnification with NIS-Elements AR

5.21.03 software. Concentrations of bacterial cells (0.20 – 2.00 μm diameter) were quantified from 15 randomly-selected view fields of 460 μm x 460 μm (211,600 μm^2) (Humphries et al. 2023).

Phytoplankton Biomass. To calculate phytoplankton biomass (as chlorophyll *a*), water (40 ml/replicate) was concentrated on to glass fiber filters (GF/Fs), then stored (-20 ^oC) in plastic scintillation vials until analysis at total (no pre-filtration), <20 μm, and <5 μm size fractions to determine the relative biomass contributions of micro-, nano- and picoplankton, respectively (Lonsdale et al. 2006; Sitta et al. 2018; Roldan-Ayala et al. 2023), following standard acetone-extraction procedures (Welschemeyer 1994) using a Turner Trilogy® fluorometer.

Phytoplankton Community Composition. Upon return to the laboratory, aliquots (3-4 ml) from each 2 L sample were qualitatively analyzed for community composition using a 5 ml Lab-Tek™ Chamber Slide and an OlymHABpus CKX53 inverted light microscope, allowing us to rapidly identify and report any harmful algal blooms (HABs). Additionally, 20 ml aliquots per replicate were fixed with Lugol's iodine solution (Sigma-Aldrich® product #1.00567) to a 3% final dilution then refrigerated (4 ^oC) until analysis. Phytoplankton community composition was determined by evaluating all preserved samples using an Olympus CKX53 inverted light microscope and a 1 ml gridded, glass Sedgewick-Rafter chamber. Individual cells (nano- and microplankton) were morphologically identified to the lowest taxonomic level possible, enumerated across the entire chamber because no blooms were observed during the study that would have warranted sub-sampling, and concentrations (cell abundances) were then calculated (LeGresley and McDermott 2010).

Genomic Analysis. To complement microscopy, both bacterial and phytoplankton species assessments were supplemented by metabarcoding analysis. Metabarcoding does not generate the detailed cell abundance and population data that comes from microscopy, however, this molecular

approach does facilitate refined taxonomic characterization of morphologically similar species. From each 9 L carboy, water samples (3 replicates) were filtered through 0.2 μm pore-size diameter polycarbonate filters (Millipore, 47 mm diameter) using peristaltic pumps at low speed. Filters containing samples were flash frozen in liquid nitrogen and stored (−80°C) until DNA extraction using a DNeasy PowerSoil Pro kit (QIAGEN) according to the manufacturer's instructions. DNA concentration from extractions was measured using a NanoDrop One Spectrophotometer (Thermo Scientific) then sent to the University of Illinois for sequencing and metabarcoding analysis. This entailed amplicon sequencing of 16S (V3 and V4 regions) and 18S rRNA (V4 region) subunits, respectively, using sequences and PCR protocols applicable to bacteria (Nubel et al. 1997; Kurobe et al. 2013), and eukaryotic phytoplankton (Gong and Marchetti 2019) followed by Illumina MiSeq platform analysis with paired-end reads (2×250 bp) (Gilbert et al. 2014).

Statistical Analysis. Datasets were tested for normality prior to analysis (Shapiro-Wilk; statskingdom.com), and any non-normally distributed datasets were log10 transformed prior to analysis. Statistical analysis entailed parametric tests using a 95% confidence interval ($\alpha = 0.05$).

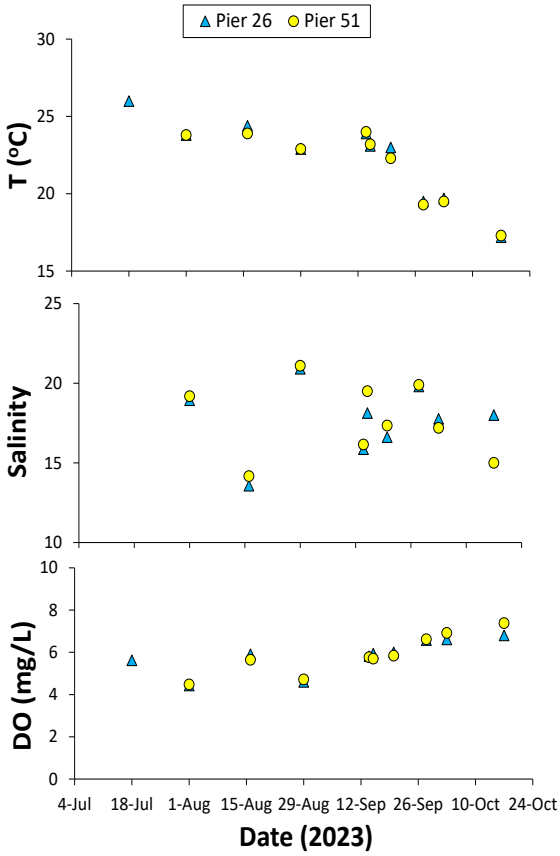

Figure 1. Time series of water quality during the study period at Piers 26 (blue triangles) and 51 (yellow circles). Parameters shown are water temperature (T, °C), salinity (dimensionless), and dissolved oxygen (DO, mg/L).

Results:

Water Quality. Both Piers 26 and 51

exhibited similar physical water quality throughout the study (**Table A1**). Water temperature was warmest at the start of data collection (18 July) at Pier 26 (26.0 ^{o}C) and GV (26.4 ^{o}C) then generally declined at both Piers 26 and 51 from August to October, consistent with seasonal cooling (**Figure 1**). The exception was 17 October, when Pier 51 had markedly fresher water and higher DO than Pier 26, despite this being a 'dry' period. During the study, wet periods occurred 16-August, 14-20 September, and 3-October (**Table A1**), and DO levels were above those associated with hypoxia (4 mg/L), with levels gradually increasing beginning mid-September (**Table A1**). Waters were moderately to highly turbid, with Secchi depths ranging 0.54 – 1.50 m corresponding to light extinction coefficients (*k*) of 3.15 – 1.13, respectively. Pier 51 typically had greater water clarity than Pier 26, but these differences were relatively minor.

Nutrients. During the study, the dissolved inorganic nitrogen (DIN) pool was dominated by ammonia+ammonium. Concentrations of nitrite+nitrate were usually low (<5 μM) (**Table 2**). By comparison, ammonia+ammonium (primarily ammonium), a key nutrient often associated with wastewater, was generally elevated throughout the study such that mean concentrations were usually >10 μM **(Figure 2**). Exceptions were at GV (18 July) and both Piers 26 and 51 on 16 August, corresponding to mean ammonia+ammonium concentrations of 9.42, 7.97, and 8.02 μM, respectively (**Figure 2; Table A2**).

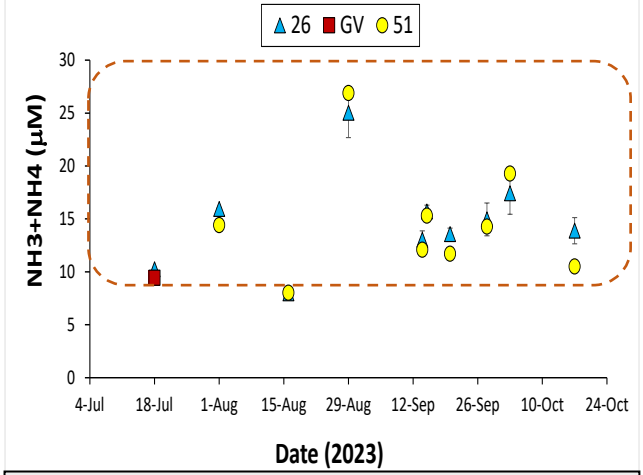

Figure 2. Mean (*n*=3, ± SE) concentrations (μM) of ammonia+ammonium during at Piers 26 (blue triangles), 51 (yellow circles), and GV (red square). Orange dashed line indicates values within ranges associated with phytoplankton growth suppression in Long Island Sound (Brown et al.

DIN concentrations were generally higher September/October than July/August,

except for 26 August when a spike in ammonia+ammonium levels was detected at both piers. This DIN increase drove a rise in the DIN to phosphate ratio (calculated from **Table A2**), potentially limiting phosphate availability to phytoplankton. Si levels were typically consistent throughout the study, with slightly lower summer concentrations measured than fall in tandem with more diatoms during August (**Tables A3-6**), presumably taking up Si during growth and frustule production.

Bacterial Abundances. Bacterial populations varied throughout the study with a peak (~88,000 cells/ml) observed on 20 September, coincident with greatest rainfall (**Figure 3**). Overall abundances, however, did not significantly correlate with rainfall amount at either site (p>0.05). Cell concentrations were generally, but not significantly, higher at Pier 51 than Pier 26.

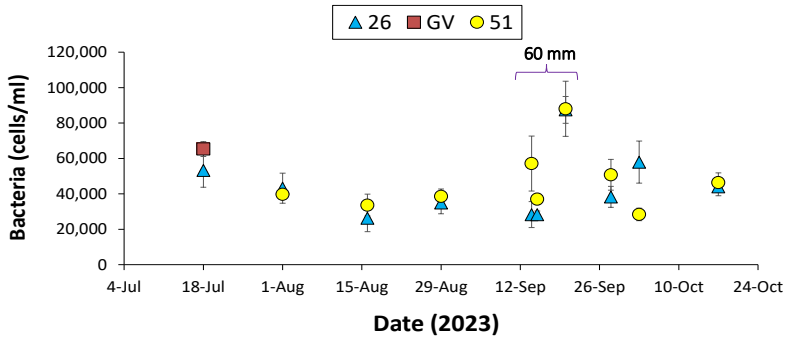

Figure 3. Mean (n=3 ± SE) bacterial abundances at Piers 26 (blue triangles), 51 (yellow circles), and GV (red square). Period of heavy rainfall (60 mm cumulative precipitation) noted by bracket.

Phytoplankton Biomass and Community Composition. Phytoplankton biomass (as chlorophyll *a*) was low (<7 µg/L) and tended to decline towards fall (**Figure 4**). The majority of phytoplankton biomass was comprised of picoplankton with a modest increase in microplankton at both Piers on 16 August and at Pier 26 on 29 August, coincident with increases in chain-forming

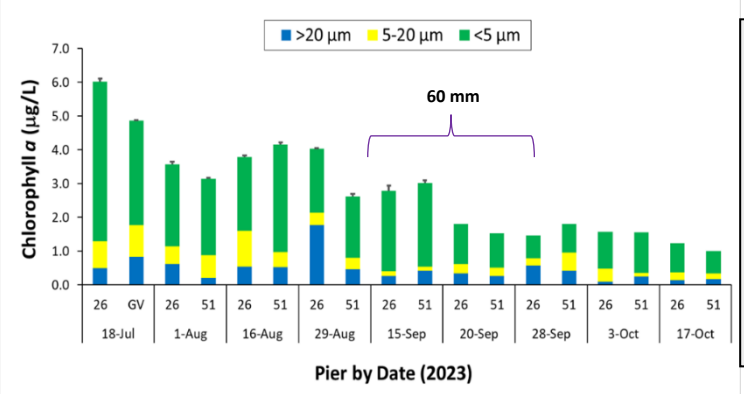

Figure 4. Mean (n=3 ± SE) chlorophyll *a* concentrations per sampling date at Piers 26, 51, and Gansevoort Peninsula (GV). Chlorophyll *a* cell size fractions (<5 µm, 5-20 µm, and >20 µm) displayed as contributions to the total. Error bars represent SE for mean total chl-*a*. The heaviest rainfall (60 mm) period is noted by brackets.

diatoms (**Table A5-6**). Chlorophyll *a* levels dropped following the September rain event and continued to decline across remaining sampling dates.

During the study period, Pier 26 exhibited the greatest overall diversity, with more diatom and dinoflagellate species (including the toxigenic organisms *Alexandrium* and *Prorocentrum cordatum*) present than at Pier 51 (**Table A3**). However, Pier 51 had comparatively more 'rare' taxa, such as silicoflagellates and chlorophytes, than Pier 26. No major phytoplankton blooms were observed (**Tables A4-6**), but concentrations of the cosmopolitan chain-forming diatom *Skeletonema costatum* were elevated on 16 August at both Pier 26 (~19,800 cell/L) and Pier 51 (69,700 cells/L) (**Tables A5-6**). Notably, the HAB-forming dinoflagellate *P. cordatum* (formerly *P. minimum*) was detected at moderately high abundances (6,500 cells/L) at Pier 26 on 17 October, along with a rise in Euglenoids (~7,200 cell/L) and the non-HAB diatom *Paralia sulcata* (~8,500 cell/L) (**Table A5**). While not at bloom levels, this warrants future surveillance because *P. cordatum* produces toxins responsible for shellfish poisoning and liver failure, making it a key species of environmental management and public health concern.

Discussion:

The similar water quality observed at both piers aligns with the fast-flowing Hudson River current, which likely transported a similar water mass across both study sites under comparable weather conditions. The exception was the noticeably fresher water at Pier 51 (15) compared to Pier 26 (18). This disparity may have been linked to freshwater inputs from the sewer system, as 2 CSO outfalls (NR 021 and NR 050) are immediately upstream from Pier 51 (**Figure A1**). According to https://openseweratlas.tumblr.com/map, the most recent data for NR 021 (2015) showed this outfall discharged 4 million gallons during that year; concurrent data are unavailable

for NR 050. During the same year, the outfall closest to Pier 26 (NC 074) discharged 5 million gallons. While these volumetric differences are relatively low (20%), our observations underscore that distance between a given sampling site and the closest upstream discharge point is important as wastewater becomes diluted by the Hudson River.

A key finding was the consistently elevated ammonium levels in the Park, coinciding with very low phytoplankton biomass and species diversity compared to other nearby estuaries such as Long Island Sound's mainstem (Santoferrara et al. 2022; Roldan-Ayala et al. 2023), northern shore (Brown et al. 2024), southern shore embayments such as Oyster Bay and Great South Bay (Greenfield et al. 2005), as well as the Peconic Bays (Lonsdale et al. 2006). This is important because HRE primary productivity has been considered to be mostly light limited (e.g., Malone 1977; Howarth et al. 2006 and others). Our measurements showed that light did indeed rapidly attenuate at both sites, as evidenced by the higher extinction coefficients within the Park compared to those calculated by our group from other regional estuaries where phytoplankton thrive (e.g., Roldan-Ayala et al. 2023; Brown et al. 2024), but ammonium levels were also exceptionally high. Ammonia+ammonium concentrations frequently exceeded 10 μM, a level associated with reduced diatom growth in both bioassay incubations (Brown et al. 2024) and environmental samples from the San Francisco Bay Delta (Glibert et al. 2016, 2022). Therefore, it is entirely possible that the consistently elevated ammonium levels observed in this study acted as a dual-stressor (with light) on the HRE microbiome, contributing to the generally low phytoplankton biomass and species richness on any given sampling date. **The discovery that the HRE ecosystem is likely co-stressed by both wastewater-N (primarily ammonia+ammonium) and light availability sheds an entirely novel insight to the NYC urban microbiome and aquatic ecosystem function.** While the precise mechanisms and the relative extent to which phytoplankton and microbial

growth was limited by ammonium and/or light was not tested here, this is an exciting research avenue that should be considered in future studies. Similarly, processes that drive HAB formation, emphasizing dinoflagellates, should also be prioritized, as evidenced by the numerous HAB species observed. While the 20 September spike in bacteria concentrations were directly associated with the most severe storm period and indicative of a CSO event, the 29 August spike in ammonia+ammonium levels occurred before the main 'wet' events. This indicates that nutrient inputs may have come from either runoff or that wastewater release was not directly in response to a CSO. Prior studies by our group also noted spikes in both dissolved organic matter and DIN during mid-October (Humphries et al. 2023; Roldan-Ayala et al. 2023) coincident with higher fecal indicator bacterial levels (Riverkeeper.com) but not necessarily with greater precipitation.

In conclusion, this study revealed that the microbial and biogeochemical processes of waters within the Park are directly influenced by the surrounding urban landscape. In particular, N-rich wastewater, as well as potentially non-point source inputs, present a pervasive stressor to the inhabiting microbiome. Results will enrich ongoing data collection and insights in to microbial diversity, biogeochemical features, and linkages with runoff that could inform ecological and climate models that enhance the resilience of NYC's waterways. Future studies should explore connections between N-rich wastewater inputs and microbial ecological processes.

Appendices:

Additional Figures

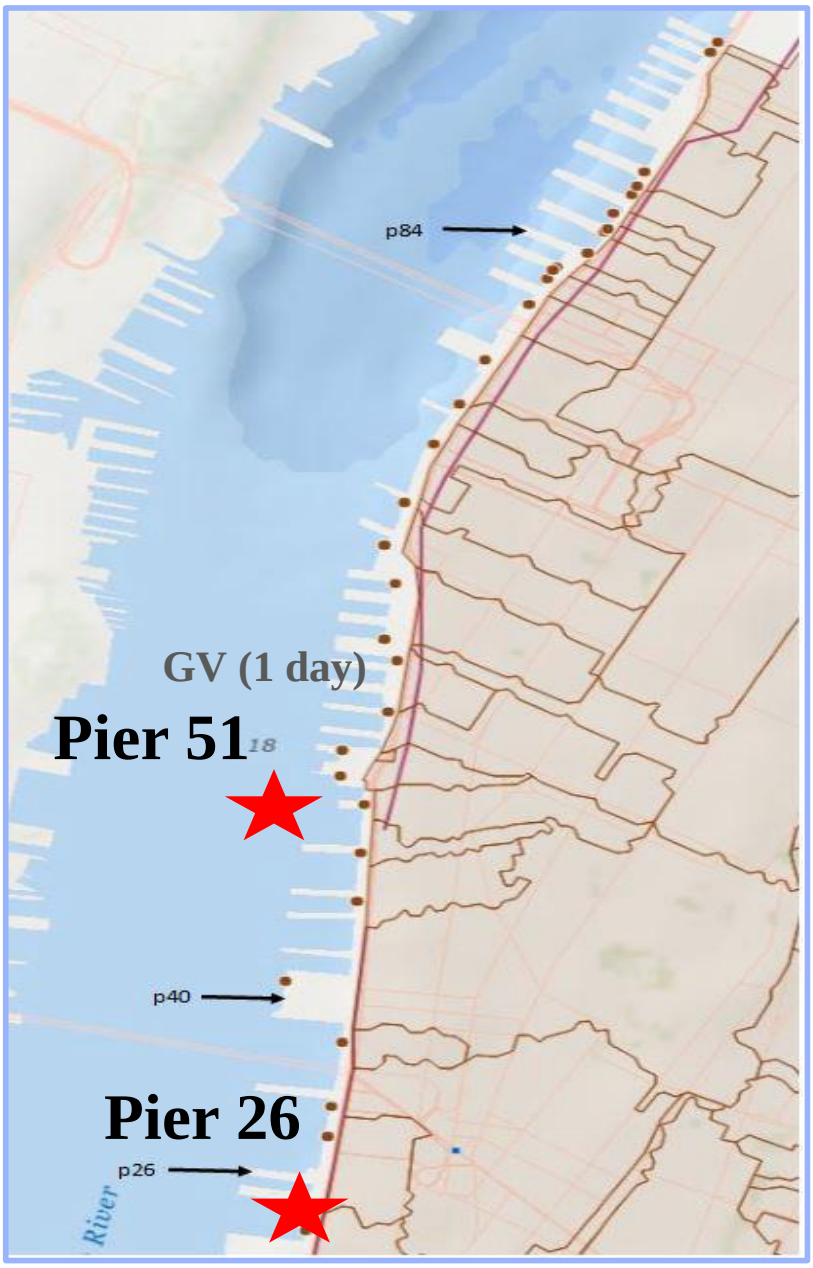

Figure A1. Map of Hudson River Park Trust's 4-mile waterfront noting study sampling sites (red stars) at Piers 26 and 51. Gansevoort (GV) Pier is noted where the first day of sampling occurred. CSO outfall locations are depicted as brown dots along the perimeter.

Tables

Table A1. Summary of water quality data for each sampling date (2023) during the study from Piers 26, 51, and Gansevoort Peninsula (GV). Parameters include water temperature (T, °C), salinity (S, dimensionless), dissolved oxygen (DO, mg/L), pH, Secchi depth (m), light extinction coefficient (*k*), cumulative 5-day precipitation (mm), and weather noting air temperature (°F/°C). Asterisk (*) indicates data leveraged from HRECOS at Pier 26, and dash '-' indicates parameter was not available for that location/site.

Date (2023)	Pier	T (°C)	S	DO (mg/L)	pH*	Secchi Depth (m)	*k*	Precip (mm)*	Weather, Air T (°F/°C)
18-Jul	26	26.0	6.67	5.62	7.6	0.54	3.15	10.9	Cloudy (82/28)
	GV	26.4	6.30	6.01	-	0.65	2.62		Cloudy (82/28)
1-Aug	26	23.8	18.93	4.43	7.6	0.55	3.09	1.8	Sunny, (71/22)
	51	23.8	19.18	4.48	-	0.60	2.83		Sunny, (71/22)
16-Aug	26	24.4	13.56	5.91	7.6	1.25	1.36	35.6	Cloudy (71/22)
	51	23.9	14.16	5.65	-	1.50	1.13		Cloudy (71/22)
29-Aug	26	22.9	20.91	4.60	7.6	0.75	2.27	10.8	Cloudy (65/18)
	51	22.9	21.10	4.72	-	0.60	2.83		Cloudy (65/18)
14-Sep	26	23.9	15.86	5.82	7.7	0.60	2.83	42.4	Cloudy (69/21)
	51	24.0	16.15	5.77	-	0.60	2.83		Cloudy (69/21)
15-Sep	26	23.1	18.13	5.94	7.8	1.00	1.70	31.0	Sunny (63/17)
	51	23.2	19.50	5.70	-	0.90	1.89		Sunny (63/17)
20-Sep	26	23.0	16.61	6.00	7.7	0.90	1.89	17.6	Sunny (68/20)
	51	22.3	17.34	5.84	-	0.90	1.89		Sunny (68/20)
28-Sep	26	19.5	19.80	6.58	7.8	0.56	3.04	11.2	Cloudy (57/14)
	51	19.3	19.90	6.62	-	0.60	2.83		Cloudy (57/14)
3-Oct	26	19.7	17.76	6.61	7.7	0.90	1.89	37.1	Sunny (76/24)
	51	19.5	17.20	6.92	-	1.00	1.70		Sunny (76/24)
17-Oct	26	17.3	18.00	6.80	8.0	1.00	1.70	7.1	Cloudy (60/16)
	51	17.3	15.00	7.38	-	1.10	1.55		Cloudy (60/16)

Table A2. Summary of mean (*n*=3) and standard error (parentheses) nutrient data for each sampling date (2023) during the study from Piers 26, 51, and Gansevoort Peninsula (GV). Parameters include nitrite+nitrate (NO2+NO3), ammonia+ammonium (NH3+NH4), orthophosphate (PO4), and silicate (SI). All concentration values are in micromoles (μM).

Date (2023)	Pier	NO2+NO3	NH3+NH4	PO4	SI
18-Jul	26	2.610 (0.074)	10.231 (0.104)	1.190 (0.064)	4.119 (0.066)
	GV	2.022 (0.247)	9.422 (0.567)	0.922 (0.053)	4.084 (0.052)
1-Aug	26	1.946 (0.006)	15.941 (0.086)	1.300 (0.106)	3.741 (0.075)
	51	1.937 (0.030)	14.418 (0.041)	0.860 (0.019)	3.504 (0.146)
16-Aug	26	3.015 (0.017)	7.976 (0.275)	1.035 (0.135)	3.917 (0.041)
	51	3.026 (0.058)	8.025 (0.542)	1.350 (0.065)	3.941 (0.012)
29-Aug	26	2.596 (0.028)	25.030 (2.341)	1.185 (0.043)	4.645 (0.031)
	51	2.527 (0.115)	26.886 (1.561)	2.723 (0.063)	4.630 (0.234)
14-Sep	26	3.357 (0.017)	13.038 (0.845)	1.025 (0.078)	4.357 (0.031)
	51	3.295 (0.232)	12.087 (1.240)	1.628 (0.095)	4.179 (0.024)
15-Sep	26	1.199 (0.196)	15.703 (0.594)	0.691 (0.009)	5.401 (0.126)
	51	1.040 (0.075)	15.299 (0.516)	0.693 (0.008)	5.366 (0.012)
20-Sep	26	3.636 (0.223)	13.562 (0.571)	0.830 (0.018)	3.917 (0.071)
	51	3.690 (0.123)	11.706 (0.865)	1.045 (0.129)	4.012 (0.012)
28-Sep	26	3.652 (0.195)	14.966 (1.551)	0.837 (0.063)	4.594 (0.054)
	51	3.517 (0.295)	14.276 (0.311)	0.838 (0.049)	4.380 (0.074)
3-Oct	26	4.475 (0.070)	17.416 (1.978)	1.155 (0.046)	3.811 (0.054)
	51	4.473 (0.092)	19.272 (1.443)	0.883 (0.153)	4.167 (0.041)
17-Oct	26	3.319 (0.012)	13.330 (1.041)	0.858 (0.058)	4.416 (0.374)
	51	3.412 (0.180)	10.493 (0.357)	0.914 (0.036)	5.020 (0.090)

Group	Species	GV	Pier 26	Pier 51
Diatoms	*Amphiprora*		X	
	Azpeitia			X
	Chaetoceros		X	X
	Coscinodiscus		X	X
	Cyclotella		X	X
	Ditylum brightwellii		X	
	Eucampia zodiacus		X	X
	Fragillaria		X	X
	Leptocylindrus sp.		X	X
	Leptocylindrus danicus		X	X
	Leptocylindrus minimus		X	X
	Lithodesmium undulatum		X	
	Melosira		X	X
	Navicula	X	X	X
	Nitzschia longissima			X
	Paralia sulcata		X	
	Pleurosigma		X	
	Pseudo-nitzshia		X	X
	Rhizosolenia			X
	Skeletonema costatum		X	X
	Suriella		X	
	Synedra	X	X	
	Thalassionema	X	X	X
	Thalassiosira	X	X	X
	Thalassiothrix			X
subtotal		*4*	*21*	*18*
Dinoflagellates	*Alexandrium*		X	
	Amphidinium		X	X
	Gymnodinium		X	
	Heterocapsa rotundata	X	X	X
	Oxyrrhis marina	X		
	Prorocentrum cordatum		X	
	Prorocentrum gracile		X	
	Prorocentrum triestinum		X	
	Protoperidinium sp.		X	
	Protoperidinium quinquecorne			X
	Scrippsiella		X	X
subtotal		*2*	*9*	*4*
Cyanobacteria	*Lyngbya*		X	
subtotal		*0*	*1*	*0*
Euglenoids	*Euglena*		X	X
subtotal		*0*	*1*	*1*
Raphidophytes	*Heterosigma akashiwo*			X
subtotal		*0*	*0*	*1*
Chlorophytes	*Scenedesmus*	X		X
subtotal		*1*	*0*	*1*
Cryptophytes	*Cryptomonas*		X	X
subtotal		*0*	*1*	*1*
Silicoflagellates	*Ebria tripartita*			X
subtotal		*0*	*0*	*1*
Microzooplankton	*Loricate ciliates*	X		X
	Non-loricate ciliates		X	X
subtotal		*1*	*1*	*2*
Mesozooplankton	*Copepod nauplii*		X	
	Unknown larvae		X	
subtotal		*0*	*2*	*0*
Total observations (alpha diversity)		**9**	**36**	**29**

Table A3. Summary of all phytoplankton species within their primary taxonomic group observed across the full study period (18 Jul-17 Oct 2023) from Gansevoort Peninsula (GV), Pier 26, and Pier 51. 'X" indicates the positive detection of a species, with observations tallied within group (subtotal) as well as overall (total), to indicate alpha diversity.

Table A4. Summary of mean (*n*=3) phytoplankton abundances (cells/L) observed on the single sampling date (2023) at Gansevoort Peninsula. Phytoplankton are listed within their major taxonomic group then species identified to the lowest taxonomic level possible.

Group	Species	18-Jul
Diatoms	*Navicula*	684
	Synedra	342
	Thalassionema	342
	Thalassiosira	3,420
Dinoflagellates	*Heterocapsa rotundata*	342
	Oxyrrhis marina	342
Microzooplankton	*Loricate ciliates*	342
Chlorophytes	*Scenedesmus*	342

Table A5. Summary of mean (*n*=3) phytoplankton abundances (cells/L) observed throughout the study (2023) at Pier 26. Phytoplankton are listed within their major taxonomic group then species identified to the lowest taxonomic level possible. Dash '-' indicates the species was not detected on that date; **bold** indicates incidences where the organism had elevated abundances.

Group	Species	18-Jul	1-Aug	16-Aug	29-Aug	15-Sep	20-Sep	28-Sep	17-Oct
Diatoms	*Amphiprora*	342	-	-	-	-	342	-	-
	Chaetoceros	-	-	-	-	-	1,026	6,154	-
	Coscinodiscus	-	342	342	1,368	-	-	-	342
	Cyclotella	-	-	342	-	-	-	2,051	-
	Ditylum brightwellii	-	-	-	-	-	-	342	-
	Eucampia zodiacus	-	1,026	-	-	7,180	-	4,103	-
	Fragillaria	-	-	-	-	342	-	-	-
	Leptocylindrus sp.	4,790	-	684	-	-	-	-	1,026
	Leptocylindrus danicus	-	-	-	-	1,368	-	342	-
	Leptocylindrus minimus	-	1,710	3,761	-	-	-	-	-
	Lithodesmium undulatum	342	-	-	-	-	-	-	-
	Melosira	-	-	-	2,393	2,393	-	3,419	684
	Navicula	342	-	342	1,026	342	-	342	1,704
	Paralia sulcata	-	-	-	2,735		-	-	**8,547**
	Pleurosigma	-	1,026	-	-	342	-	-	342
	Pseudo-nitzshia	-	-	-	-	-	-	1,026	-
	Rhizosolenia	-	-	-	-	-	-	-	342
	Skeletonema costatum	5,130	3,461	**19,830**	-	**10,254**	-	2,735	-
	Suriella	342	-	-	-	342	-	-	-
	Synedra	-	-	-	-	-	-	-	1,026
	Thalassionema	684	-	-	-	-	-	342	-
	Thalassiosira	3,077	2,393	2,393	3,077	2,393	2,393	6,154	4,786
Dinoflagellates	*Alexandrium*	-	-	-	-	-	342	-	-
	Amphidinium	-	-	-	-	-	342	-	-
	Gymnodinium	-	-	-	342	-	-	-	-
	Heterocapsa rotundata	-	-	-	-	-	-	-	2,051
	Oxyrrhis marina	-	-	-	-	-	-	-	-
	Prorocentrum cordatum	342	-	342	342	-	342	-	**6,496**
	Prorocentrum gracile	-	-	-	-	342	-	-	684
	Prorocentrum triestinum	-	684	-	-	-	-	-	1,709
	Protoperidinium sp.	-	-	-	-	-	342	-	-
	Scrippsiella	-	-	-	-	-	-	-	684
Euglenoids	*Euglena*	342	1,026	1,026	1,026	342	342	-	**7,180**
Cryptophytes	*Cryptomonas*	684	-	-	-	342	-	-	-
Cyanobacteria	*Lyngbya*	342	-	-	-	-	-	-	-
Microzooplankton	*Non-loricate ciliates*	-	342	-	-	-	-	-	-
Mesozooplankton	*Copepod nauplii*	-	342	-	-	-	-	-	-
	Unknown larvae	-	1,026	-	-	-	-	-	-

Table A6. Summary of mean (*n*=3) phytoplankton abundances (cells/L) observed throughout the study (2023) at Pier 51. Phytoplankton are listed within their major taxonomic group then species identified to the lowest taxonomic level possible. Dash '-' indicates the species was not detected on that date; **bold** indicates incidences where the organism had elevated abundances.

Group	Species	1-Aug	16-Aug	29-Aug	15-Sep	20-Sep	28-Sep	17-Oct
Diatoms	*Azpeitia*	-	-	-	-	-	342	-
	Chaetoceros	-	-	-	1,709	-	5,470	-
	Coscinodiscus	-	342	2,564	-	-	-	-
	Cyclotella	2,735	-	-	-	-	4,103	-
	Eucampia zodiacus	-	-	-	4,444	684	2,051	-
	Fragillaria	-	342	-	342	-	-	-
	Leptocylindrus sp.	-	-	-	-	2,393	-	3,077
	Leptocylindrus danicus	-	-	-	2,051	-	-	-
	Leptocylindrus minimus	-	4,786	-	-	-	-	-
	Lithodesmium undulatum	-	-	-	-	-	-	-
	Melosira	-	-	513	-	684	-	684
	Navicula	1,026	1,368	-	342	1,368	1,368	-
	Nitzschia longissima	-	-	513	-	-	-	-
	Pseudo-nitzshia	-	-	-	-	-	684	-
	Rhizosolenia	-	-	513	-	-	-	-
	Skeletonema costatum	12,308	**69,744**	3,590	-	1,368	2,051	2,393
	Suriella	-	-	-	-	-	-	342
	Synedra	-	-	-	-	-	-	-
	Thalassionema	5,128	684	-	-	-	684	-
	Thalassiosira	1,368	2,051	2,051	3,419	1,368	4,444	2,051
	Thalassiothrix	-	-	-	-	-	342	-
Dinoflagellates	*Amphidinium*	-	-	-	684	-	-	-
	Heterocapsa rotundata	-	-	-	-	-	-	684
	Prorocentrum cordatum	-	-	-	-	342	-	342
	Protoperidinium quinquecorne	-	-	-	342	-	-	-
	Scrippsiella	-	-	-	-	-	-	342
Euglenoids	*Euglena*	-	684	513	342	-	-	1,709
Raphidophytes	*Heterosigma akashiwo*	-	342	-	-	-	-	-
Chlorophytes	*Scenedesmus*	-	342	-	-	-	-	-
Cryptophytes	*Cryptomonas*	-	1,026	-	-	342	-	342
Silicoflagellates	*Ebria tripartita*	-	342	-	-	-	342	342
Microzooplankton	*Loricate ciliates*	-	-	-	-	684	-	-
	Non-loricate ciliates	-	-	-	1,026	-	-	-

References:

Brown, M., Ambrosone, M., Turner, K. J., Humphries, G., Tzortziou, M., Anglès, S., Panzeca, C. and Greenfield, D. I. 2024. Phytoplankton assemblage responses to nitrogen following COVID-19 stay-in-place orders in Western Long Island Sound (New York/Connecticut). Marine Environmental Research. 196: 106371.

Gilbert, J. A., Jansson, J. K. and Knight, R. 2014. The Earth Microbiome Project: successes and aspirations. BMC Biology 12: 69.

Glibert, P.M., Wilkerson, F.P., Dugdale, R.C., Raven, J.A., Dupont, C.L., Leavitt, P.R., Parker, A.E., Burkholder, J.M. and Kana, T.M. 2016. Phytoplankton community interactions and environmental sensitivity in coastal and offshore habitats. Oikos 125(8): 1134-1143.

Glibert, P.M., Wilkerson, F.P., Dugdale, R.C. and Parker, A.E. 2022. Ecosystem recovery in progress? Initial nutrient and phytoplankton response to nitrogen reduction from sewage treatment upgrade in the San Francisco Bay Delta. Nitrogen 3(4): 569-591.

Gong, W. and Marchetti, A. 2019. Estimation of 18S gene copy number in marine eukaryotic plankton using a next-generation sequencing approach. Frontiers in Marine Science 2019.00219.

Grasshoff, K. K., Kremling, K. and Ehrhardt, M. 1999. Methods of Seawater Analysis, Wiley-VCH. 599 pp.

Greenfield, D. I., Lonsdale, D. J. and Cerrato, R. M. 2005. Linking phytoplankton community composition with juvenile-phase growth in the northern quahog *Mercenaria mercenaria* (L.). Estuaries and Coasts. 28 (2) 241-251.

Hales, B., van Geen, A., Takahashi, T. 2004. High-frequency measurement of seawater chemistry: Flow-injection analysis of macronutrients. Limnology and Oceanography: Methods 2: 91-101.

HEP (Hudson River Estuary Program). 2020. State of the Hudson, The Hudson River Estuary Program, NY-NJ Harbor and Estuary Program and NEIWPCC. New York. 97 pp.

Herve, V., Leroy, B., Da Silva Pires, A. and Lopez, P.J. 2018. Aquatic urban ecology at the scale of a capital: community structure and interactions in street gutters. ISME Journal 12: 253–66.

Howarth, R. W., Marino, D., Swaney, P. and Boyer, E. 2006. Wastewater and watershed influences on primary productivity and oxygen dynamics in the lower Hudson River Estuary. Pp. 121-139 *In*: Levinton, J. S. and Waldman, J. R. (eds) The Hudson River Estuary. Cambridge University Press.

Humphries, G., Espinosa, J., Ambrosone, M., Roldan-Ayala, Z., Tzortziou, M., Goes, J. and Greenfield, D. I. 2023. Transitions in nitrogen and organic matter form and concentration

correspond to bacterial population dynamics in a hypoxic urban estuary. Biogeochemistry 163 (2): 219-243.

(IPCC) Intergovernmental Panel on Climate Change. 2018. Report to the United Nations.

Kurobe, T., Baxa, D. V., Mioni, C. E., Kudela, R. M., Smythe, T. R., Waller, S., Chapman, A. D. and The, S. J. 2013. Identification of harmful cyanobacteria in the Sacramento-San Joaquin Delta and Clear Lake, California, by DNA barcoding. SpringerPlus Article 491.

LeGresley, M. and McDermott, G. 2010. Counting chamber methods for quantitative phytoplankton analysis - haemocytometer, Palmer-Maloney cell and Sedgewick-Rafter cell. Intergovernmental Oceanographic Commission manuals and guides 55: Microscopic and molecular methods for quantitative phytoplankton analysis. UNESCO, 25-30.

Lonsdale, D. J., Greenfield, D. I., Hillebrand, E. H., Nuzzi, R. and Taylor, G. T. 2006. Contrasting microplanktonic composition in two coastal embayments (Long Island, New York). Journal of Plankton Research 28: 891-905.

Malone, T.C. 1977. Environmental regulation of phytoplankton productivity in the Lower Hudson River Estuary. Estuarine and Coastal Marine Science. 5: 157-171.

Nubel, U., Garcia-Pichel, F., and Muyzer, G. 1997. PCR primers to amplify 16S rRNA genes from cyanobacteria. Applied and Environmental Microbiology 63: 3327-3332.

Porter, K. and Feig, Y. S. 1980. The use of DAPI for identifying and counting aquatic microfloral. Limnology and Oceanography 25(5): 943-948.

Riverkeeper, 2015. How's the water? Fecal Contamination in the Hudson River and its Tributaries. http://www.riverkeeper.org/wp
content/uploads/2015/06/Riverkeeper_WQReport_2015_Final.pdf

Roldan-Ayala, Z, Arnott, S. A., Ambrosone, M., Espinosa, J., Humphries, G., Tzortziou, M., Goes, J. and Greenfield, D. I. 2023. The influences of phenology, spatial distribution, and nitrogen form on Long Island Sound phytoplankton biomass and taxonomic composition. Estuarine, Coastal and Shelf Science 292: 108451.

Rosenzweig, B., Montalto, F. A., Orton, P., Kaatz, J., Maher, N., Kleyman, J., Chen, Z., Sanderson, E., Adhikari, N., McPhearson, T. and Herreros-Cantis, P. 2024. NPCC4: Climate change and New York City's flood risk. Annals of the New York Academy of Sciences. 1539: 127-184.

Santoferrara, L. F., McManus, G. B., Greenfield, D. I., and Smith, S. A. 2022. Microbial

communities (bacteria, archaea, and eukaryotes) in a temperate estuary during seasonal hypoxia. Aquatic Microbial Ecology. 88: 61-79.

Sitta, K., Callahan, T., Doll, C., Mortensen, R., Reed M., and Greenfield, D. I. 2018. The influences of nitrogen form and zooplankton grazing on phytoplankton assemblages in two coastal southeastern systems. Limnology and Oceanography 63: 2523-2544.

Steinberg, N., Suszkowski, D. J., Clark, L. and Way, J. 2004. Health of the Harbor: The first comprehensive look at the state of the NY/NJ harbor estuary. A report to the NY/NJ Harbor Estuary Program. Hudson River Foundation, New York, NY. 82 pp

Vaudrey, J. M. 2017. New York City's impact on Long Island Sound water quality. PhD Thesis University of Connecticut.

Wang, J. 2014. Combined sewer overflows (CSOs) impact on water quality and environmental ecosystem in the Harlem River. Journal of Environmental Protection 5: 1373-1389.

Welschmeyer, N. A. 1994. Fluorometric analysis of chlorophyll *a* in the presence of chlorophyll *b* and phaeopigments. Limnology and Oceanography 39: 1985-1992.

Whitney, M. M. and Vlahos, P. 2021. Reducing hypoxia in an urban estuary despite climate warming. Environmental Science and Technology 55: 941-951.

Acknowledgements:

I would like to thank CUNY's Office of Research and Hudson River Park Trust for supporting this work. Many thanks to Moonmoon Ahmed, the student involved with this this research, for her dedication and hard work. I also thank Greenfield lab members Mariapaola Ambrosone, Georgie Humphries, Nicolle Navaretta, Nick Russell, and Sequoia Kessler for helping with sampling during the 2023 field season. Finally, thanks to the many Park staff for helping with sampling, transportation, and many other aspects of this pilot study.